Microfluidics and Nanofluidics (2020) 24:29
https://doi.org/10.1007/s10404-020-02334-6

RESEARCH PAPER

Acoustic bubble-based bidirectional micropump

Yuan Gao[1] · Mengren Wu[1] · Yang Lin[1] · Weiqi Zhao[1] · Jie Xu[1]

Received: 9 December 2019 / Accepted: 16 March 2020

Abstract
Efficient transportation of fluids and microparticles is an important capability in many medical and biological applications. In this article, an efficient bi-directional micropump using microcavity-trapped acoustic bubbles is studied. With acoustic actuation, a controllable microstreaming net flow is generated inside a microchannel by the oscillating bubbles. Based on theory and experimental results, different sized microbubbles have different resonant frequencies. Thus, by oppositely placing the different sized microbubbles, the flow direction can be switched via altering the frequency. The pumping flow rate can be tuned by adjusting the input voltage and can achieve as high as 1600 nl/min with high stability. Furthermore, the bi-directional pumping ability is also proved using blood-mimicking fluid (BMF), allowing for on-chip high-viscosity fluid pumping. In the end, the proposed device is employed in pumping *Escherichia coli* bacteria, indicating that the micropump is capable of pumping cells without damaging them. This inexpensive, portable and biocompatible acoustic bubble-based bi-directional pump for transporting fluids and particles has great potential to integrate with other on-chip platforms for multiple biological and chemical applications, such as drug delivery, cell separation, and chemical analysis.

Keywords Microfluidics · Microstreaming · Acoustic bubble · Bi-directional micropump · *E. coli*

1 Introduction

Microfluidic pumps capable of transporting small volumes of fluid are widely applied in engineering research and life science studies. Comparing with the conventional syringe pumps, microfluidic pumps have the capability of combining with other on-chips functional units to realize portable micro total analysis systems (μTAS). Due to the requirement of efficient and precise flow control for microfluidic applications, many types of pumps have been explored, such as electric (Kumar et al. 2016; Vafaie et al. 2016), magnetic (Johnson and Borkholder 2016; Tang et al. 2018; Zhang et al. 2018), acoustic (Girardo et al. 2008; Johari et al. 2011) and mechanical energy-based pumps (Wang et al. 2017; Forouzandeh et al. 2019). Among these pumps, microelectrothermal pumps have been used in driving high conductivity biofluid (Gao and Li 2018; Salari and Dalton 2019); MEMS-based micropumps are applied in drug delivery and transport fluid (Nisar et al. 2008; Cobo et al. 2015); and implantable micropumps are developed for periodic drug delivery and some of them have successfully been implanted in the human body to treat anabolic osteoporosis (Farra et al. 2012; Johnson and Borkholder 2016). Although these pumps are efficient to many biological and chemical applications, there still exist challenges including complex fabrication processes, expensive materials and setup, and limited flow control. To address these critical problems for micropumps, acoustic bubbles and acoustically oscillating solid structures have emerged as promising tools for precise control of the flow in lab-on-a-chip applications.

Acoustically oscillating solid structures can produce acoustic streaming, which gained much attention recently due to their great potential in a wide variety of lab-on-a-chip applications. For instance, oscillating sharp edges have been studied for fluid mixing (Huang et al. 2013, 2015), fluid bi-directional transportation (Mohanty et al. 2019), particle trapping (Leibacher et al. 2015), and nanoparticle synthesing (Huang et al. 2019). Likewise, acoustically oscillating bubbles can also produce streaming around the bubbles, a

Electronic supplementary material The online version of this article (doi:https://doi.org/10.1007/s10404-020-02334-6) contains supplementary material, which is available to authorized users.

✉ Jie Xu
jiexu@uic.edu

[1] Department of Mechanical and Industrial Engineering, University of Illinois At Chicago, Chicago, IL 60607, USA

Published online: 02 April 2020

phenomenon termed microstreaming in the literature. Microstreaming is due to a non-linear second-order effect (Marmottant and Hilgenfeldt 2003) and can also be harnessed for various lab-on-a-chip applications (Hashmi et al. 2012). Especially in recent years, many innovative acoustic bubble-based devices have been developed for flow control and particle manipulation. For example, Ryu et al. produced a directional microstreaming flow by placing a capillary tube above an excited acoustic bubble (Ryu et al. 2010). Later, a micropump based on lateral cavity acoustic transducer (LCAT) was developed for pumping liquids in a microchannel (Tovar et al. 2011). Many effective bubble-based micromixers have also been investigated to mix fluid (Ahmed et al. 2009; Wang et al. 2011). For particle manipulation, a bubble based separator and switch (Patel et al. 2014), a rotational microorganism manipulation technique (Xu et al. 2013; Ahmed et al. 2016) and a cell lyser and drug transporter have been introduced (Marmottant and Hilgenfeldt 2003; Marmottant et al. 2006). However, to the best of our knowledge, among these acoustic bubble-based applications, a micropump that can pump fluids in multiple directions in a microfluidic device has never been reported, which is an important function for many applications. In this work, we applied acoustic bubbles for bi-directional pumping with the advantages of low-cost, simple fabrication process, biocompatibility and precise controllability.

It is of great importance to generate bubbles and maintain them in desired positions for the acoustic bubble-based applications. Hashimi et al. utilized a micromilled asymmetric teardrop-shaped cavity to trap a three-dimensional air bubble in an open fluid domain (Hashmi et al. 2013). Lin et al. also explored the method to generate 3D microbubbles inside a microchannel using nanostructures fabricated by two-photon polymerization technique (Lin et al. 2019a, b). Electrolysis is also used to generate and control small bubbles using a Pt electrode on the surface (Chung and Cho 2009). As a liquid handing tool, micropipette has been used to inject air bubbles in a droplet and a hydrophobic plate is used for transporting and pumping (Chung and Cho 2008; Ryu et al. 2010). Using a microliter syringe, researchers successfully created an acoustically excited bubble by simultaneously injecting gas and liquid into a microchannel for biomedical applications (Rogers and Neild 2011; Tandiono et al. 2012). With the help of vertical and lateral cavities within sidewalls, air–liquid interface can be created inside the microchannel by slowly injecting liquid into an air-filled microchannel (Ahmed et al. 2016; Garg et al. 2018). In this study, we develop a method via creating cavity structures inside a recirculated microchannel to trap air–liquid interfaces for generating bi-directional acoustic microstreaming flow for pumping fluids and biological samples (Fig. 1). Based on theoretical calculation and experimental results, the flow direction and flow rates are accurately controlled in the microchannel by controlling the applied frequency and voltage applied to the piezoelectric actuator. We also investigate the stability of the bubbles and their influence on pumping performance. Furthermore, we implement the acoustic bubble-based pumping device for driving blood-mimicking fluid (BMF) and *Escherichia coli*, demonstrating potential real-world applications of bi-directional fluid flow control.

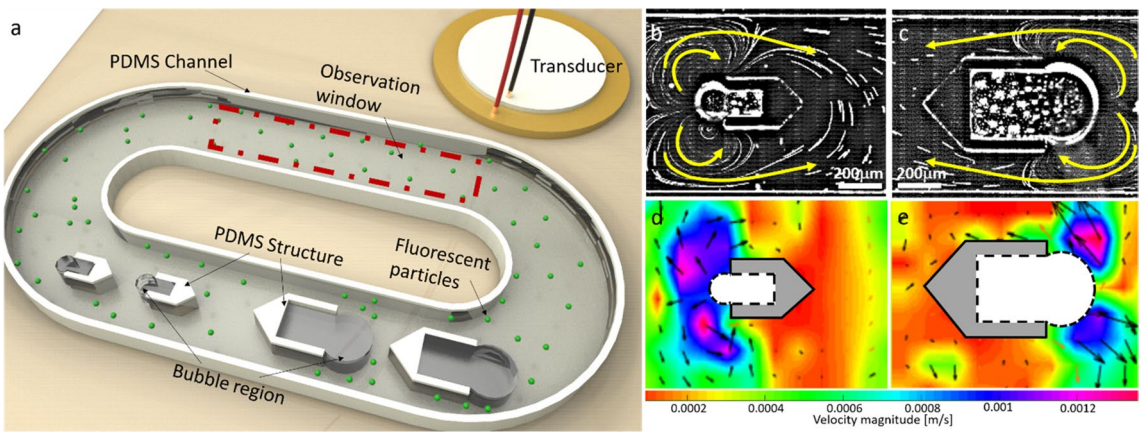

Fig. 1 **a** Configuration of the acoustic-based bi-directional micropump device and piezoelectric transducer; **b**, **c** acoustic microstreaming flow induced by different sized bubbles: small-sized bubble and large-sized bubble, respectively; **d**, **e** the velocity profile inside the microchannel of the bubble based micropump device given by particle image velocimetry (PIV) measuring technique. The actuation voltage is 5 Vpp and the frequencies are 24 kHz and 19 kHz, respectively

2 Experimental section

2.1 Microfabrication

The Polydimethylsiloxane (PDMS) microchannel with pre-designed cavity structures was fabricated using standard soft lithography and mold replica technique (Xia and Whitesides 1998). SU-8 2050 (Microchem Corp., USA) photoresist was spin-coated on a 4-inch silicon wafer to produce the desired master mold, followed by UV exposure and development. Then, a mixture of a PDMS (Sylgard 184, Dow Corning) with 10:1 base to curing agent ratio was prepared and placed in a vacuum desiccator (Bel-Art Scienceware, NJ) for removing air bubbles. After that, the PDMS mixture was poured onto the silicon master mold and placed into oven to bake at 65 °C for 1 h. When curing is completed, the PDMS was peeled off gently and punched with one inlet and one outlet.

2.2 Experimental setups

To avoid randomly trapped bubbles at the corner of the rectangle-shaped channel, we designed a ring-shaped recirculated channel to demonstrate the pumped flow. The width and depth of the ring-shaped recirculated channel are 800 µm and 100 µm, respectively. Two small (120 µm × 175 µm) and two large (320 µm × 275 µm) cavity structures were oppositely placed in the center of microchannel as shown in Fig. 2. The center to center distance between the two small cavity structures, the two neighboring large and small cavity structures, and the two large cavity structures are 700 µm, 950 µm and 1000 µm, respectively. The height of the structure (100 µm) was designed to be the same as the depth of the microchannel. After standard soft lithography and mold replica process, the PDMS microchannel was bonded on glass microscope slides (75 mm × 50 mm × 0.90–1.10 mm, Corning®, USA) using 1.5 min plasma treatment.

To activate the device, a 27 mm piezoelectric transducer (Vktech, USA) was adhered to this glass slice covered by ARcare® 90,445 (Adhesives Research, Glen Rock, PA) plastic double-sided adhesive tape. The piezoelectric transducer was driven by a function generator (DG1022U; Rigol Technologies Inc., Beijing, China) and amplified (25 ×) by a voltage amplifier (Tegam 2350, Tegam Inc., Madison, OH). The device is mounted on the stage of an inverted microscope (Nikon Eclipse Ti-S, Nikon Instrument Inc), monitored by a high-speed camera (Phantom Miro M310, Vision Research Inc., USA) and illuminated by a fluorescence illuminator (X-cite 120, Lumen Dynamics, Ontario, Canada).

2.3 Flow characterization by microparticle image velocimetry (µPIV)

To quantitively characterize the velocity field around the microbubbles, a widely used processing technique, microparticle image velocimetry (µPIV) was applied. The 2 µm flow-tracing fluorescent particles were used for µPIV process. The device was placed on an inverted microscope equipped with a fluorescence illuminator and a high-speed camera. Once the pumping flow was generated in the device, the high-speed camera started to capture images with high resolution (1280 × 720). Images were then analyzed by open-source Matlab-based software—PIVLab (Thielicke and Stamhuis 2014). In pre-processing phase, the region of interest (ROI) was first

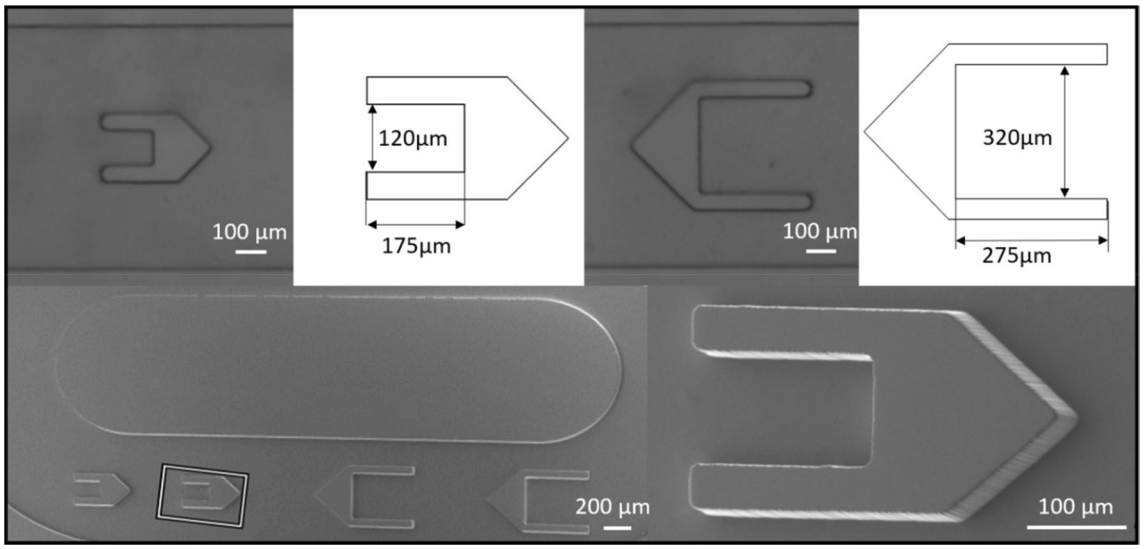

Fig. 2 Dimensions and SEM images of the small cavity structure and large cavity structure

defined, as shown in Fig. 1d and e. The image contrast was then enhanced using a contrast limited adaptive histogram equalization (CLAHE). Images were cross-correlated using 50% overlapped interrogation area with two passes to quantify the displacement between the pairs of successive images. During post-processing, a smoothing procedure and velocity limits were used to remove noise vectors; the appearance was set as HSV (hue, saturation, value) color map. As a result, the velocity field around the bubble was obtained. Although the velocity may be not very accurate due to the bubble oscillation, the characterization of the velocity distribution was demonstrated by μPIV measurement.

2.4 Sample preparation

To demonstrate the particle transportation and visualize the microstreaming flow direction generated by the micropump device, DI water with 2.0 μm diameter green fluorescent microparticles (Fluoro-Max dyed polystyrene microspheres, Thermo Fisher Scientific, Waltham, MA) was used as fluid media.

To validate the micropump device with biological samples without damaging live cells, *Escherichia coli* was chosen as a sample cell type to be examined in the micropump device. The *E. coli* cells were grown in Tryptic Soy Broth culture medium at 37 °C shaking incubator. Once the *E. coli* concentration kept constant at 8.0×10^8 cell mL^{-1}, they were combined with 0.4% Trypan blue for assessing cell viability, followed by injecting cells into chips for experimentation.

3 Theory

3.1 Microstreaming flow

When a microbubble or air–liquid interface is oscillating by mechanical perturbation in the fluid media, a circulating flow pattern is formed resulting in microstreaming. There would be inner vortices (primary vortices) in the boundary layer, which would drive outer vortices (secondary vortices) over a scale similar to several radii of the bubble (Lane 1955). Microstreaming flow around a bubble can be described as (Marmottant et al. 2006)

$$u_i = u_s \sin(\Delta\emptyset)\left[\frac{1}{2}S_{ij}^{W}\left(\frac{R_b}{a}\right) - \frac{1}{4}M_{ij}^{D,W}\left(\frac{R_b}{a}\right) - \frac{1}{2}M_{ij}^{H,W}\left(\frac{R_b}{a}\right)\right] \quad (1)$$

where ΔØ denotes the phase difference between the two modes of the bubble's motion: (1) a dipole (translational harmonic vibration) and (2) a monopole (volume pulsation/radial motion). Translational vibration means that the bubble moves back-and-forth along a line while the volume pulsation means the expanding and contracting motion of the bubble. S_{ij}^{W},$M_{ij}^{D,W}$ and $M_{ij}^{H,W}$ are the Green's function of a point force, a dipole and the hexadecapole singularity of the bubble center (Pozrikidis 1992; Longuet-Higgins 1998). R_b is the radius of the bubble. u_s is the streaming velocity of a vibrating bubble, which is given by:

$$u_s = {u_0}^2/\omega\ell \quad (2)$$

where u_0 is the amplitude of the oscillatory flow, ω is the angular frequency and ℓ is the length of the gradient of u_0 along with the boundary layer (Nyborg 1958; Lighthill 1978; Squires and Quake 2005).

The microstreaming occurs due to the first order pulsatile flow generated by pulsation of the microbubble, which induced the second-order streaming flow due to the inertial force and the viscous force. This pumping phenomenon requires that the Reynolds number near the bubbles is large enough for the second-order streaming flow to be dominated by inertial force (Dijkink et al. 2006; Tovar et al. 2011). The Reynold's numbers near the bubble is given by:

$$\mathrm{Re} = 2R_b\omega A/\nu \quad (3)$$

where A is the maximum oscillation amplitude of liquid–air interface. ν is the kinematic viscosity of the liquid.

3.2 Microstreaming and frequency

According to Eq. 1, the microstreaming flow pattern is associated with the oscillation mode of the microbubble, which is affected by the acoustic force and gas compressibility. The strong microstreaming flow is produced when the applied frequency is close to the bubble's resonant frequency. The linear resonant frequency f of a free-standing spherical bubble can be presented by Minnaert eigenfrequency equation (Minnaert 1933).

$$f_0 = \frac{1}{2\pi R_b}\sqrt{\frac{3\gamma P_0}{\rho}} \quad (4)$$

Here, γ is the polytropic exponent, which is 1.4 for an air bubble (Crum 1983). P_0 is the ambient pressure and ρ denotes the density of the liquid. The equation shows that the resonant frequency of the bubble is related to the radius of the bubble and thus the microstreaming is strongly dependent on the driving frequency and the radius of the bubble. Although the theoretical calculation is valid only for free-standing spherical bubbles, it estimates that the resonant frequencies of the large bubble and small bubbles used in our experiments are 16.3 kHz and 31.0 kHz, respectively,

which provides a starting point for the experimental efforts discussed in the next section.

3.3 Acoustic radiation force and drag force

Under acoustic actuation, microparticles suspended in a fluid may experience acoustic radiation force and drag force. Whether the movement of microparticles is dominated by acoustic streaming induced Stokes' drag force or secondary radiation force depends on the size, as well as the properties of microparticles and the surrounding fluid, which has been explained in several theoretical and numerical studies (Qiu et al. 2019). At low Reynolds number, the drag force is given by Stokes' law, which can be described as:

$$F_{\mathrm{D}} = -6\pi\mu R_{\mathrm{p}} v \tag{5}$$

where μ is the viscosity of the fluid media, R_{p} is the radius of the particle, υ is the relative velocity of the fluid and particles.

The time-averaged product of the gradient in the acoustic pressure and in the fluctuation of bubble volume produces a type of acoustic radiation force (Dayton et al. 1997). The radiation force is a second-order non-linear force acting on a particle, which is induced by the nonuniform momentum around the particle. The primary acoustic radiation force in the acoustic wave can be expressed as (Yosioka and Kawasima 1955):

$$F_{\mathrm{PRF}} = 4\pi k {R_{\mathrm{p}}}^3 E_{\mathrm{s}} K_{\mathrm{s}} \sin(2\mathrm{kz}) \tag{6}$$

where k is the acoustic wave number, z is the position of the particle relative to the pressure node, E_{s} is the energy density (Groschl 1998). K_{s} is the acoustophoretic coefficient and is expressed by (Yosioka and Kawasima 1955):

$$K_{\mathrm{s}} = \frac{1}{3}\left[\frac{5\tilde{\rho} - 2}{2\tilde{\rho} + 1} - \frac{1}{\tilde{\rho}\,\sigma^2}\right] \tag{7}$$

where $\tilde{\rho}$ denotes the density ratio of the particle to the media, σ denotes the sound speed ratio of particle to the media. When acoustophoretic coefficient becomes negative ($K_{\mathrm{s}} < 0$), the particle will move toward the pressure antinodes. Conversely, particles will move toward the pressure nodes when acoustophoretic coefficient is positive.

Particles move to pressure nodes due to the primary acoustic force. Once the particles aggregate, the interparticle force becomes more and more significant. The secondary radiation force is a short-range effect and can keep the particles oscillating in a certain range of distances, which is given by (Coakley and Nyborg 1978):

$$F_{\mathrm{SRF}} = 4\pi\rho_{\mathrm{l}} \frac{\rho_{\mathrm{l}} - \rho_{\mathrm{p}}}{\rho_{\mathrm{l}} + 2\rho_{\mathrm{p}}} \frac{R^4 R_{\mathrm{p}}^3}{d^5} \omega^2 \xi^2 \tag{8}$$

where ρ_{l} is the density of the liquid, ρ_{p} is the density of the particle, d denotes the distance between the center of the bubble and center of the particle. ω presents the applied frequency, and ξ is the oscillation amplitude of the bubble.

In this work, to demonstrate the pumping flow and acoustic microstreaming pattern, the particle size is selected as 2 μm, which is dominated by the drag force rather than secondary radiation force. Therefore, the pumping flow rate can be estimated by tracing the trajectory of the particles.

4 Results and discussion

4.1 Mechanism of bubble-based bidirectional micropump

The working mechanism of this acoustic bubble-based bidirectional micropump is shown in Fig. 1a. Due to surface tension, air was passively trapped inside cavity structures and liquid–air interfaces were generated when liquid flowed through the microchannel. As mentioned previously, when exposed to the acoustic field activated by an external piezoelectric transducer, the air–liquid interfaces oscillate, and the microstreaming flow was generated as the driving frequency gets close to the resonant frequency of the bubbles. The different sized cavities, therefore, were designed for creating different sized bubbles with different resonant frequencies. The different sized cavity structures oppositely faced each other in the center of the lower part of the channel. Thereby the opposite directional microstreaming flow was achieved by adjusting the applied frequency.

To characterize the microstreaming pattern around the air–liquid interface, we injected green fluorescent particles with deionized (DI) water into the channel using a syringe pump. After that, the inlet and outlet of the recirculated channel were sealed by tape to make sure there is no pressure difference between them. Once the fluid achieved equilibrium state, the acoustic wave was applied to actuate the micropump and a strong directional microstreaming flow occurred around two different cavity structures at their resonant frequencies respectively, which is schematically presented in Fig. 1b and c. Additionally, to quantitatively characterize the velocity field of the microstreaming inside the channel, a microparticle image velocimetry (μPIV) technique was used. The velocity vector distributions at the frequencies of 19 kHz and 24 kHz around two different structures are shown in Fig. 1d and e. It is worth noting that the microstreaming flow pattern can be affected by frequency, shape and volume of bubbles, as well as surround structures

(Tho et al. 2007; Wang et al. 2013). In this study, at frequencies of 24 kHz and 19 kHz, the flow direction is dominated by the two symmetric vortices generated on the two sides of oscillating bubbles. As marked in Fig. 1b and c, the two symmetric vortices drew the fluid to the bubble and pass the structural gap to the backside of the bubbles/structures.

4.2 Pumping performance

4.2.1 Pumping behavior

To further demonstrate the pumping behavior, we took images from a defined observation window, located at the center of the upper channel (Fig. 1a), to show the movement of microparticles. Figure 3 shows the movement of microparticles transported at the frequency of 24 kHz and 19 kHz at different frames in the defined observation window. Specifically, with the frequency of 24 kHz, the small bubbles were actuated and the microparticles were moving from right to left with the flow. Conversely, the large bubbles were excited and particles were pumped from left to right achieved by tuning the frequency to 19 kHz. The results not only demonstrated particle transport but also proved that the selective flow control in a microchannel can be realized using this acoustic bubble-based bi-directional pump device.

4.2.2 Frequency sweeping

In this part, we investigate the relationship between the bubble's resonant frequency and pumping performance. To obtain the optimal pumping performance for the two directions at the constant voltage, the frequency was swept around theoretical resonant frequencies with a 1 kHz increment at a constant 5 Vpp actuation voltage. The results of the flow rate versus frequency are presented in Fig. 4a. The flow rate was mapped by tracing the trajectory of the suspended particles in the defined observation window. When particles moved along the positive x-axis in the defined observation window (clockwise direction), the large microbubbles were actuated by the acoustic force with the positive velocity. On the contrary, the particles moved in the opposite direction when small microbubbles were activated. As can be seen, the peak flow rate occurs when the driving frequencies are 19 kHz and 24 kHz, respectively. During the experiment, the pumping flow direction can be instantly switched by changing the frequency from 19 to 24 kHz, or 24 kHz to 19 kHz (Video 1). Based on this result, 19 kHz and 24 kHz are considered as the optimal working frequencies that were used for the following studies.

4.2.3 Effect of driving voltage

To further characterize the pumping behavior, we explored the influence of the applied voltage on the pumping performance. During the experiment, we applied input voltage ranging from 1 to 7 Vpp with 1 Vpp increment to actuate small-sized bubbles and large-sized bubbles at 24 kHz and 19 kHz respectively (Video 2 and 3). As shown in Fig. 4b and c, with increasing voltage, the pumping flow rate increased significantly. For the small bubbles induced counterclockwise flow, the flow rate rises from 50 nl/min to 1200 nl/min. For the large bubbles induced clockwise flow,

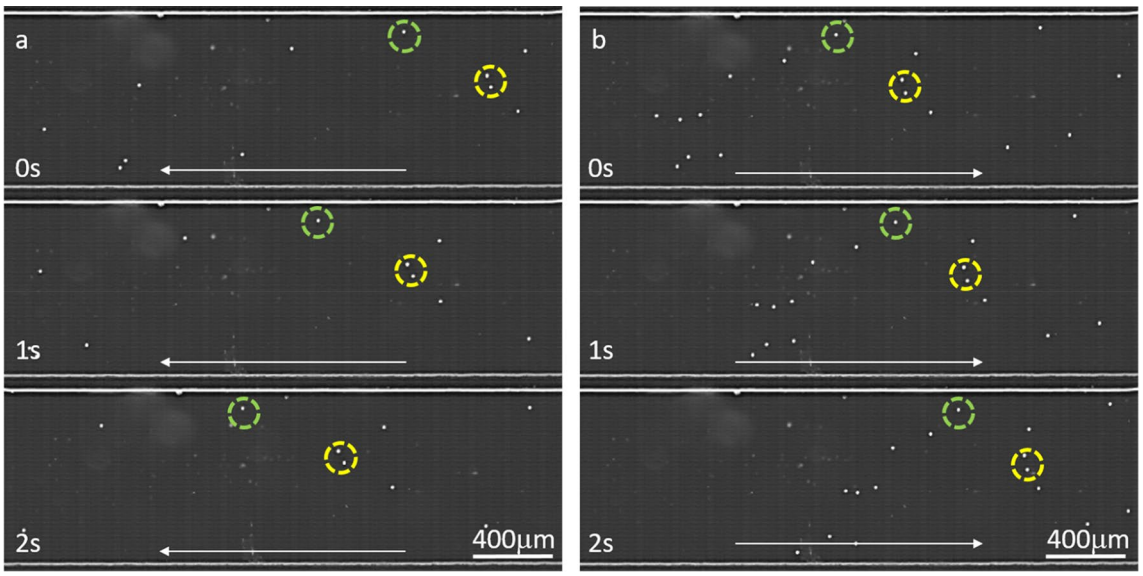

Fig. 3 Movement of the microparticles in the observation window (refer to Fig. 1). **a** Microparticles moved toward left when the small bubbles were activated at 24 kHz; **b** Microparticles moved toward the right when the large bubbles were actuated at 19 kHz

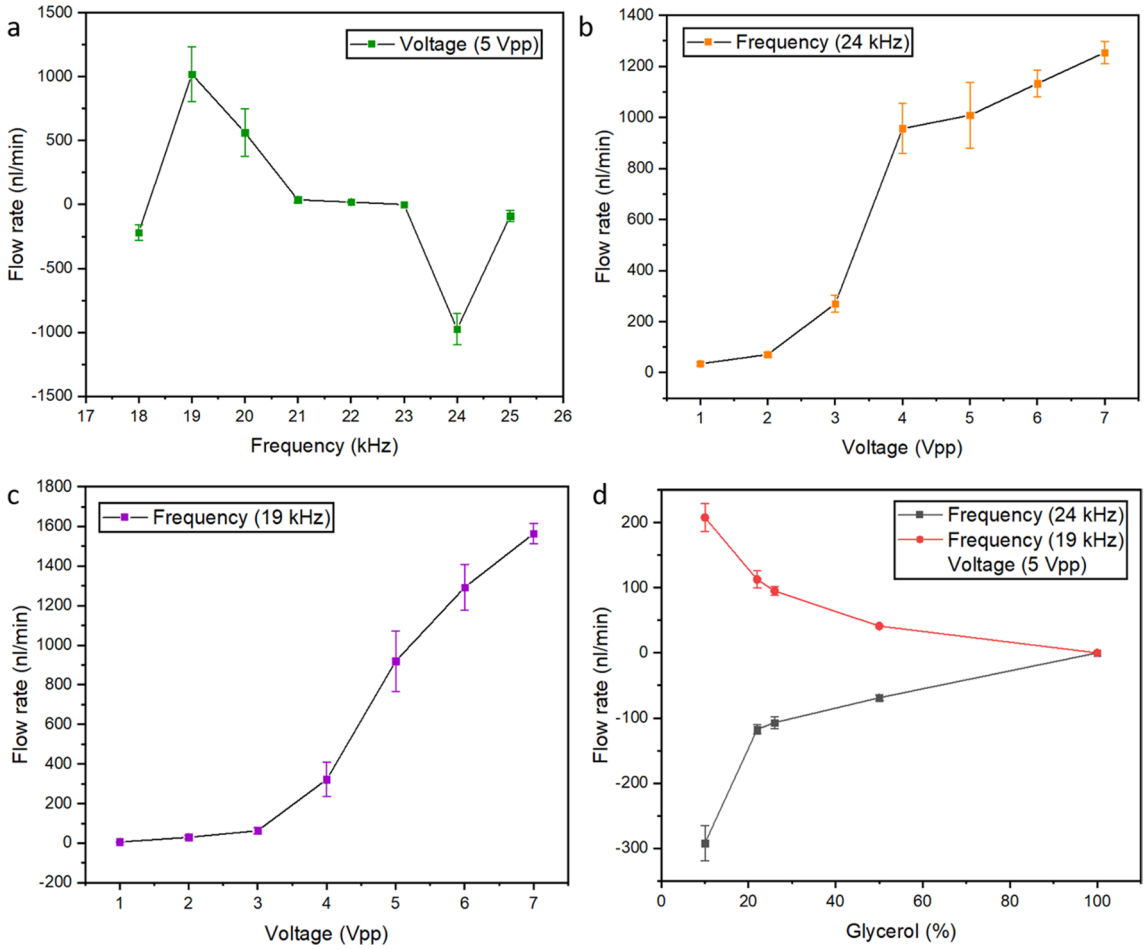

Fig. 4 **a** Plot of pumping flow rate versus driving frequency; **b**, **c** pumping flow rate versus the voltage, illustrating the flow rate increased with increasing voltage; at a frequency of 24 kHz and 19 kHz, respectively; **d** plot of the pumping flow rate versus glycerol concentration at 5 Vpp demonstrating high viscosity fluid pumping. The pumping flow rate decreased with the increase of viscosity

the flow rate can achieve from 20 nl/min to 1600 nl/min. These experimental results are reasonable since oscillating bubble amplitudes increase with the voltage, and based on the stream function of the microbubbles, they will generate stronger microstreaming flow to produce a higher flow rate.

4.3 Pumping test with blood-mimicking fluid (BMF)

Pumping biological fluid samples is a necessary step for many lab-on-a-chip and point-of-care applications. Blood as the most important body fluid has been widely studied and processed for various microfluidic applications, including drug delivery, cell separation, and disease diagnosis. Due to the similar properties with blood and being non-hazadous, blood-mimicking fluid (BMF) is usually used for simulating blood in early-stage biomedical experiments. To realize realistic blood flow mimicking, the dynamic viscosity of BMF should be similar to human blood. Here, we conducted experiments to further investigate the capability of our pumping system in biological samples using blood-mimicking fluid.

At a constant voltage (5 Vpp) and frequencies (24 kHz and 19 kHz), the pumping performance was studied by altering the viscosity of the pumping liquid. According to a recent study on human blood viscosity (Yousif et al. 2011), we added glycerol into DI water to adjust the viscosity and made the blood-mimicking fluid. During the experiment, glycerol and water mixture with different viscosities were injected into the channel respectively. As shown in Fig. 4d, the micropump is capable of driving up to 50% glycerol/water mixture, which is 8 times more viscous than water. Additionally, the flow rate decreases with increasing glycerol percentage. The result proved that this bi-directional pumping device has a great potential for various biological fluid sample transportation, such as plasma (10% glycerol), whole blood (22% glycerol) and platelets (26% glycerol) (Bosart and Snoddy 1927).

4.4 Cell viability test

To further demonstrate the application of the pump with biological samples, the pump was tested by driving *E. coli* cells in the flow. During the experiment, by tuning the applied frequency, the direction of pumping *E. coli* cells can be switched rapidly. Once the applied frequency changed from 19 to 24 kHz, the *E. coli* cells were instantly pumped from clockwise direction to counterclockwise direction. When the acoustic actuation is off, it was observed that *E. coli* cells stop moving immediately. Thus, the position of *E. coli* can be transported and controlled easily by switching frequency and stopping actuation, demonstrating the high controllability of the bi-directional micropump. In addition, to prove its performance for pumping *E. coli*, it is important to know that whether the pumped *E. coli* cells are still viable since the cells could be damaged under strong forces. The viability of the pumped *E. coli* cells was tested with 4% Trypan blue solution, which can stain non-viable cells through the damaged cell membrane. Figure 5a and b show cell viability before and after 10 min actuation of the micropump. The cells highlighted by a yellow circle demonstrate a living cell and the cell marked by a red circle indicates a dead one. To quantify the cell numbers and viability, we used a hemocytometer to count the live and dead cells. The viability of the cells was calculated by Eq. 9.

$$\text{Viability}\,(\%) = \frac{\text{Total number of viable cells}}{\text{Total number of cells}} \times 100\% \qquad (9)$$

Figure 5c shows that the cell viability before acoustic pumping was 94.2% and the cell viability in the micropump remained 91.8% after 10 min acoustic actuation of the pump. From these results, we can conclude that the bi-directional micropump does not cause perceptible damage to the cells after acoustic excitation, which makes it suitable for handling biological samples for various experiments.

5 Conclusion

In this study, a novel acoustic bubble-based bi-directional micropump was demonstrated for lab-on-a-chip applications. We fabricated different-sized oppositely-facing cavity structures inside the microchannel using soft lithography technique to generate microbubbles. Based on the theoretical calculation and frequency sweeping results, we were able to find the resonant frequencies for the bubbles of two different sizes, which were 19 kHz and 24 kHz for large and small bubbles, respectively. Actuated around the resonant frequencies, a directional microstreaming flow was generated around the oscillating bubbles. Since large bubbles and small bubbles were arranged oppositely, the flow direction can be switched when altering the driving frequency. To the best of our knowledge, this is the first-time exploration of acoustic bubble-based bi-directional pumping and their potential applications in microchannels. Specifically, the microstreaming flow was created from right to left in the upper channel when the small bubbles are activated at 24 kHz. With applying the frequency of 19 kHz, the microstreaming flow switched from left to right. To visualize and quantify the flow, 2 µm fluorescent microparticles were used as tracer particles in DI water. With increasing actuation voltage, we observed that the pumping effect increases and the flow rate achieved as high as 1600 nl/min at 7 Vpp. We further investigated the pumping performance in pumping blood-mimicking fluid (BMF). The results demonstrate that the pumping device has great potential in pumping biological samples including whole blood, blood plasma and blood cells, with a trade-off of decreasing in pumping flow rate when the viscosity of fluid increases. We also tested the device for pumping live microorganisms (*E. coli*). The result indicates that *E. coli* cells can be successfully pumped in the microchannel, and the device has a minimum impact on the viability of *E. coli*. Overall, our bi-directional micropump

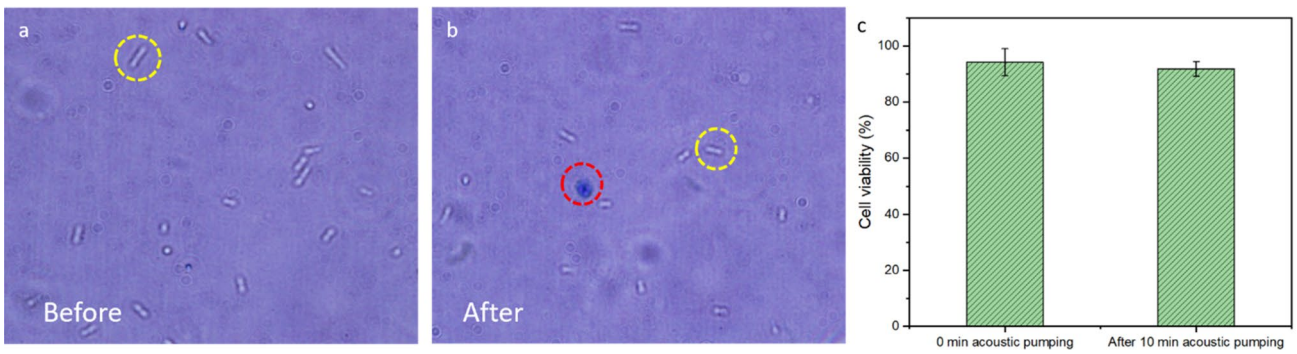

Fig. 5 After acoustic excitation, most *E. coli* cells were still alive. The cells highlighted in a yellow circle demonstrates a living cell; the cell marked by a red circle indicates a dead one. The *E. coli* cell viability was evaluated at **a** 0 min; **b** 10 min; **c** cell viability test results before and after 10 min acoustic pumping (color figue online)

shows great promise in realizing useful lab-on-a-chip applications. In the future, we plan to further explore various types of fluids, such as urine and saliva, and integrate the micropump with upstream (sample preparation) and downstream (sample analysis) microfluidic functions to realize fully integrated lab-on-a-chip systems.

Admittedly, the common problems associated with bubble based platforms still exist. For example, the size of the bubble in the microchannel could change in time, which could result in an undesired change of bubble's resonant frequency for long-term operation (Huang et al. 2012). In future, several techniques could be explored to further improve bubble stability, such as supplying constant back pressure for the bubbles (Gong et al. 2016), and 3D-print armors for the bubbles (Bertin et al. 2017; Lin et al. 2019a, b).

Acknowledgements This work was supported by an Early Career Faculty grant from NASA's Space Technology Research Grants Program (80NSSC17K0522). Yuan Gao acknowledges financial support from Sigma Xi Grants-in-Aid of Research program (G2018100198272403).

References

Ahmed D, Mao XL, Shi JJ, Juluri BK, Huang TJ (2009) A millisecond micromixer via single-bubble-based acoustic streaming. Lab Chip 9(18):2738–2741

Ahmed D, Ozcelik A, Bojanala N, Nama N, Upadhyay A, Chen YC, Hanna-Rose W, Huang TJ (2016) Rotational manipulation of single cells and organisms using acoustic waves. Nat Commun 7:11085

Bertin N, Spelman TA, Combriat T, Hue H, Stephan O, Lauga E, Marmottant P (2017) Bubble-based acoustic micropropulsors: active surfaces and mixers. Lab Chip 17(8):1515–1528

Bosart L, Snoddy A (1927) New Glycerol Tables1. Ind Eng Chem 19(4):506–510

Chung SK, Cho SK (2008) On-chip manipulation of objects using mobile oscillating bubbles. J Micromech Microeng 18(12):125024

Chung SK, Cho SK (2009) 3-D manipulation of millimeter- and micro-sized objects using an acoustically excited oscillating bubble. Microfluid Nanofluid 6(2):261–265

Coakley WT, Nyborg WL (1978) Cavitation: dynamics of gas bubbles; applications, ultrasound: its applications in medicine and biology, vol 3. Elsevier, New York, pp 77–159

Cobo A, Sheybani R, Meng E (2015) MEMS: enabled drug delivery systems. Adv Healthc Mater 4(7):969–982

Crum LA (1983) The polytropic exponent of gas contained within air bubbles pulsating in a liquid. J Acoust Soc Am 73(1):116–120

Dayton PA, Morgan KE, Klibanov ALS, Brandenburger G, Nightingale KR, Ferrara KW (1997) A preliminary evaluation of the effects of primary and secondary radiation forces on acoustic contrast agents. IEEE Trans Ultrason Ferroelectr Freq Control 44(6):1264–1277

Dijkink RJ, van der Dennen JP, Ohl CD, Prosperetti A (2006) The 'acoustic scallop': a bubble-powered actuator. J Micromech Microeng 16(8):1653–1659

Farra R, Sheppard NF, McCabe L, Neer RM, Anderson JM, Santini JT, Cima MJ, Langer R (2012) First-in-Human testing of a wirelessly controlled drug delivery microchip. Sci Transl Med 4(122):122–121

Forouzandeh F, Zhu XX, Alfadhel A, Ding B, Walton JP, Cormier D, Frisina RD, Borkholder DA (2019) A nanoliter resolution implantable micropump for murine inner ear drug delivery. J Control Release 298:27–37

Gao XB, Li YX (2018) Biofluid pumping and mixing by an AC electrothermal micropump embedded with a spiral microelectrode pair in a cylindrical microchannel. Electrophoresis 39(24):3156–3170

Garg N, Westerhof TM, Liu V, Liu R, Nelson EL, Lee AP (2018) Whole-blood sorting, enrichment and in situ immunolabeling of cellular subsets using acoustic microstreaming. Microsyst Nanoeng 4:17085

Girardo S, Cecchini M, Beltram F, Cingolani R, Pisignano D (2008) Polydimethylsiloxane-$LiNbO_3$ surface acoustic wave micropump devices for fluid control into microchannels. Lab Chip 8(9):1557–1563

Gong H, Woolley AT, Nordin GP (2016) High density 3D printed microfluidic valves, pumps, and multiplexers. Lab Chip 16(13):2450–2458

Groschl M (1998) Ultrasonic separation of suspended particles—part I: fundamentals. Acustica 84(3):432–447

Hashmi A, Heiman G, Yu G, Lewis M, Kwon HJ, Xu J (2013) Oscillating bubbles in teardrop cavities for microflow control. Microfluid Nanofluid 14(3–4):591–596

Hashmi A, Yu G, Reilly-Collette M, Heiman G, Xu J (2012) Oscillating bubbles: a versatile tool for lab on a chip applications. Lab Chip 12(21):4216–4227

Huang PH, Lapsley MI, Ahmed D, Chen YC, Wang L, Huang TJ (2012) A single-layer, planar, optofluidic switch powered by acoustically driven, oscillating microbubbles. Appl Phys Lett 101(14):1414101

Huang PH, Ren LQ, Nama N, Li SX, Li P, Yao XL, Cuento RA, Wei CH, Chen YC, Xie YL, Nawaz AA, Alevy YG, Holtzman MJ, Mccoy JP, Levinec SJ, Huang TJ (2015) An acoustofluidic sputum liquefier. Lab Chip 15(15):3125–3131

Huang PH, Xie YL, Ahmed D, Rufo J, Nama N, Chen YC, Chan CY, Huang TJ (2013) An acoustofluidic micromixer based on oscillating sidewall sharp-edges. Lab Chip 13(19):3847–3852

Huang PH, Zhao SG, Bachman H, Nama N, Li ZS, Chen CY, Yang SJ, Wu MX, Zhang SP, Huang TJ (2019) Acoustofluidic synthesis of particulate nanomaterials. Adv Sci 6(19):1970113

Johari J, Yunas J, Hamzah AA, Majlis BY (2011) Piezoelectric micropump with nanoliter per minute flow for drug delivery systems. Sains Malaysiana 40(3):275–281

Johnson DG, Borkholder DA (2016) Towards an implantable, low flow micropump that uses no power in the blocked-flow state. Micromachines 7(6):99

Kumar N, George D, Sajeesh P, Manivannan PV, Sen AK (2016) Development of a solenoid actuated planar valveless micropump with single and multiple inlet-outlet arrangements. J Micromech Microeng 26(7):075013

Lane C (1955) Acoustical streaming in the vicinity of a sphere. J Acoust Soc Am 27(6):1082–1086

Leibacher I, Hahn P, Dual J (2015) Acoustophoretic cell and particle trapping on microfluidic sharp edges. Microfluid Nanofluid 19(4):923–933

Lighthill J (1978) Acoustic streaming. J Sound Vib 61(3):391–418

Lin Y, Gao C, Gao Y, Wu MR, Yazdi AA, Xu J (2019a) Acoustofluidic micromixer on lab-on-a-foil devices. Sensors Actuators B Chem 287:312–319

Lin Y, Gao Y, Wu MR, Zhou R, Chung DY, Caraveo G, Xu J (2019b) Acoustofluidic stick-and-play micropump built on foil for single-cell trapping. Lab Chip 19(18):3045–3053

Longuet-Higgins MS (1998) Viscous streaming from an oscillating spherical bubble. Proc R Soc Lond Ser A 454(1970):725–742

Marmottant P, Hilgenfeldt S (2003) Controlled vesicle deformation and lysis by single oscillating bubbles. Nature 423(6936):153–156

Marmottant P, Raven JP, Gardeniers H, Bomer JG, Hilgenfeldt S (2006) Microfluidics with ultrasound-driven bubbles. J Fluid Mech 568:109–118

Minnaert M (1933) XVI. On musical air-bubbles and the sounds of running water. Lond Edinb Dublin Philosoph Mag J Sci 16(104):235–248

Mohanty S, de Cumis US, Solsona M, Misra S (2019) Bi-directional transportation of micro-agents induced by symmetry-broken acoustic streaming. AIP Adv 9(3):035352

Nisar A, AftuIpurkar N, Mahaisavariya B, Tuantranont A (2008) MEMS-based micropumps in drug delivery and biomedical applications. Sensors and Actuators B-Chemical 130(2):917–942

Nyborg WL (1958) Acoustic streaming near a boundary. J Acoust Soc Am 30(4):329–339

Patel MV, Nanayakkara IA, Simon MG, Lee AP (2014) Cavity-induced microstreaming for simultaneous on-chip pumping and size-based separation of cells and particles. Lab Chip 14(19):3860–3872

Pozrikidis C (1992) Boundary integral and singularity methods for linearized viscous flow. Cambridge University Press, Cambridge

Qiu W, Karlsen JT, Bruus H, Augustsson P (2019) Experimental characterization of acoustic streaming in gradients of density and compressibility. Phys Rev Appl 11(2):024018

Rogers P, Neild A (2011) Selective particle trapping using an oscillating microbubble. Lab Chip 11(21):3710–3715

Ryu K, Chung SK, Cho SK (2010) Micropumping by an acoustically excited oscillating bubble for automated implantable microfluidic devices. Jala 15(3):163–171

Salari A, Dalton C (2019) Simultaneous pumping and mixing of biological fluids in a double-array electrothermal microfluidic device. Micromachines 10(2):92

Squires TM, Quake SR (2005) Microfluidics: fluid physics at the nanoliter scale. Rev Mod Phys 77(3):977–1026

Tandiono T, Ow DSW, Driessen L, Chin CSH, Klaseboer E, Choo ABH, Ohl SW, Ohl CD (2012) Sonolysis of *Escherichia coli* and *Pichia pastoris* in microfluidics. Lab Chip 12(4):780–786

Tang SY, Zhang XC, Sun SS, Yuan D, Zhao QB, Yan S, Deng L, Yun GL, Zhang J, Zhang SW, Li WH (2018) Versatile microfluidic platforms enabled by novel magnetorheological elastomer microactuators. Adv Funct Mater 28(8):1705484

Thielicke W, Stamhuis E (2014) PIVlab–towards user-friendly, affordable and accurate digital particle image velocimetry in MATLAB. J Open Res Softw 2(1):e30

Tho P, Manasseh R, Ooi A (2007) Cavitation microstreaming patterns in single and multiple bubble systems. J Fluid Mech 576:191–233

Tovar AR, Patel MV, Lee AP (2011) Lateral air cavities for microfluidic pumping with the use of acoustic energy. Microfluid Nanofluid 10(6):1269–1278

Vafaie RH, Ghavifekr HB, Van Lintel H, Brugger J, Renaud P (2016) Bi-directional ACET micropump for on-chip biological applications. Electrophoresis 37(5–6):719–726

Wang C, Rallabandi B, Hilgenfeldt S (2013) Frequency dependence and frequency control of microbubble streaming flows. Phys Fluids 25(2):022002

Wang SS, Huang XY, Yang C (2011) Mixing enhancement for high viscous fluids in a microfluidic chamber. Lab Chip 11(12):2081–2087

Wang XR, Jiang HW, Chen YC, Qiao X, Dong L (2017) Microblower-based microfluidic pump. Sens Actuators A Phys 253:27–34

Xia YN, Whitesides GM (1998) Soft lithography. Annu Rev Mater Sci 28:153–184

Xu YH, Hashmi A, Yu G, Lu XN, Kwon HJ, Chen XL, Xu J (2013) Microbubble array for on-chip worm processing. Appl Phys Lett 102(16):023702

Yosioka K, Kawasima Y (1955) Acoustic radiation pressure on a compressible sphere. Acta Acust Unit Acust 5(3):167–173

Yousif MY, Holdsworth DW, Poepping TL (2011) A blood-mimicking fluid for particle image velocimetry with silicone vascular models. Exp Fluids 50(3):769–774

Zhang SZ, Wang Y, Lavrijsen R, Onck PR, den Toonder JMJ (2018) Versatile microfluidic flow generated by moulded magnetic artificial cilia. Sens Actuators B Chem 263:614–624